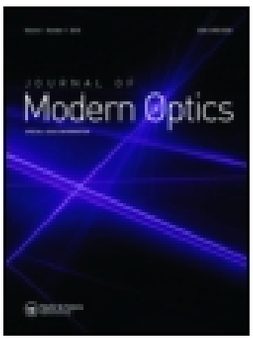

Journal of Modern Optics

ISSN: 0950-0340 (Print) 1362-3044 (Online) Journal homepage: https://www.tandfonline.com/loi/tmop20

On-axis phase-only computer-generated holograms based on a minimal etching process

Uriel Levy , David Mendlovic & Zeev Zalevsky

To cite this article: Uriel Levy , David Mendlovic & Zeev Zalevsky (1998) On-axis phase-only computer-generated holograms based on a minimal etching process, Journal of Modern Optics, 45:7, 1437-1449, DOI: 10.1080/09500349808230639

To link to this article: https://doi.org/10.1080/09500349808230639

JOURNAL OF MODERN OPTICS, 1998, VOL. 45, NO. 7, 1437–1449

On-axis phase-only computer-generated holograms based on a minimal etching process

URIEL LEVY, DAVID MENDLOVIC and ZEEV ZALEVSKY
Tel-Aviv University, Faculty of Engineering, 69978 Tel-Aviv, Israel

(*Received 25 October 1997; revision received 20 January 1998*)

Abstract. Diffractive optical elements able to generate on-axis (zero-order) phase as well as amplitude distributions are described. The proposed elements are surface-relief plates, that is phase-only elements, that are based on concepts of computer-generated masks followed by lithographic and etching processes. The proposed encoding method assumes variable spatial partitioning of the cell and a fixed phase value allocated to each subcell. This method requires the minimal number of etching levels needed for full representation of the wave front, that is three, but can be applied with improved efficiency using more etching levels. The reconstructed amplitude and phase distributions contain some noise owing to the encoding process. Discussion of the error sources is given.

1. Introduction

Many approaches for achieving synthetic holographic elements have been proposed in the last three decades. For example the methods proposed by Brown and Lohmann [1] and Lohmann and Paris [2], who invented the first computerized encoding method of holograms, and later by Lee [3], Burckhardt [4], Hsueh and Sawchuck [5], Gallagher and Bucklew [6] and Matic and Hensen [7]. A common feature of all these methods is that the reconstructed image is displayed off axis. The off-axis reconstruction is usually undesired owing to high sensitivity to wavelength deviation. Moreover, the complexity of the optical set-up needed is significantly increased. In addition, these methods were based on an amplitude-only mask (although the usage of a binary phase-only filter is possible), and therefore suffer from relatively low light efficiency. Owing to the above phase-only filter which reconstructs the desired amplitude and phase distributions in the zero diffraction order is desired.

The first phase-only filter approach was suggested by Lessem *et al.* [8]. They used a sawtooth carrier in order to encode both phase and amplitude information. However, the reconstruction was still achieved off axis. Several other methods based on a phase-only filter in which the reconstruction is achieved in the zero diffraction order were suggested [9, 10]. All these methods and their disadvantages (such as high noise and the high depth resolution needed) have been described in a previous paper [11] which also suggested an improved approach for achieving a phase-only zero-order computer-generated hologram. This method is based on fixed partition of the element cells. Each partition is etched to a 'grey-level' (continuous value) depth. However, although the required spatial resolution is relatively low, the depth resolution needed according to this approach is very high

0950–0340/98 $12·00

and therefore many etching steps are needed. This might be a significant fabrication limitation. All the above methods can be combined with the error diffusion approach [12] in order to reduce the quantization noise within the reconstructed image.

In addition, there are several iterative approaches such as the iterative Fourier transform algorithm (IFTA) [13] and simulated annealing [14]. These are iterative approaches and therefore are time consuming and computationally complex. Moreover, the IFTA must use phase and/or amplitude freedom which might be undesired for several applications, such as correlation.

The motivation of this project is to increase the variety of approaches for computer-generated holograms. The niche that this project addresses is rapid computation, simple fabrication needs and obtaining a phase-only mask and on-axis reconstruction.

In the following, we offer a new encoding approach which enables the use of a minimal number of phase values, that is three. Therefore only two etching steps (with identical depth) are needed and the production process is simplified significantly. However, high spatial bandwidth is now needed. Hence, the proposed method is perfect when high spatial resolution and low depth resolution are available. An analysis of the proposed approach is given in section 2. Comprehensive discussion of the various error terms and efficiency calculation is given in section 3. Computer simulations that prove the capability of the proposed encoding approach are shown in section 4.

2. The encoding procedure

The proposed encoding procedure is based on presenting the mask plane as being composed of macropixels. Each macropixel consists of three regions etched to a fixed and different phase value (0, $2\pi/3$, $4\pi/3$). The aim of the subdivision is to enable the encoding of amplitude as well as phase information by surface-relief elements. Indeed, this is the phase-only on-axis equivalent of the Lee–Burckhardt method. The sizes of these regions are used as a degree of freedom; therefore two degrees of freedom are available for each cell (macropixel). The procedure relies on utilizing surface-relief elements that may be fabricated using common lithographic and etching techniques. The obtained beam is generated with a relatively high light efficiency. These elements can be replicated easily and are cost effective. The encoding approach requires very low depth resolution, although the needed spatial resolution is rather high.

A two-dimensional top view construction of the encoded cell is illustrated in figure 1, and a typical depth profile is shown schematically in figure 2. The λf coefficient is necessary since optical instead of mathematical transformation is involved. Figure 3 explains the encoding method by a complex plane representation of the macrocell's value. It is obvious that every complex value can be represented by its (0°, 120°, 240°) three projections. Each cell in this representation is encoded by three sections with variable width that are associated with the length of the complex value projections. Two free parameters exist in this representation, namely W_1 and W_2 (shown in figure 2), which are the widths of each subcell of the cell (m, n), while W_3 is the complementary section. These free parameters will be shown to be able to encode the required phase and amplitude of the cell. The mathematical expression for the mask represented by all cells is given by

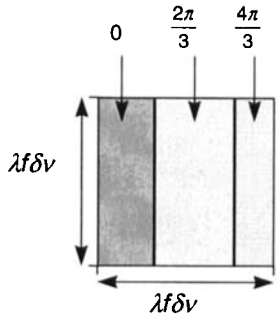

Figure 1. Top view of a cell.

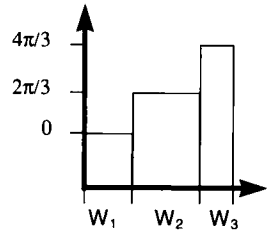

Figure 2. Depth profile of a cell.

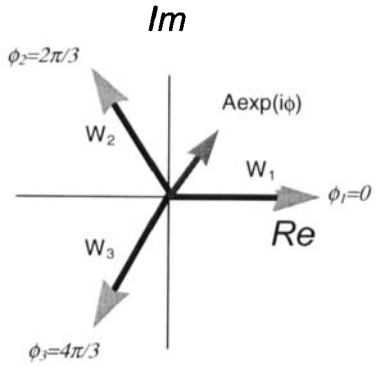

Figure 3. The complex-plane representation.

$$H(\nu_x,\nu_y)=\sum_m\sum_n \operatorname{rect}\left(\frac{\nu_y}{\delta\nu}\right)\left\{\operatorname{rect}\left(\frac{\nu_x}{W_1\,\delta\nu}\right)*\delta\left[\nu_x-\left(m-\frac{W_2+W_3}{2}\right)\delta\nu\right]\delta(\nu_y)\right.$$
$$+\operatorname{rect}\left(\frac{\nu_x}{W_2\,\delta\nu}\right)*\exp\left(\frac{\mathrm{i}2\pi}{3}\right)\delta\left[\nu_x-\left(m-\frac{W_3-W_1}{2}\right)\delta\nu\right]\delta(\nu_y)$$
$$\left.+\operatorname{rect}\left(\frac{\nu_x}{W_3\,\delta\nu}\right)*\exp\left(\frac{\mathrm{i}4\pi}{3}\right)\delta\left[\nu_x-\left(m-\frac{W_1-W_2}{2}\right)\delta\nu\right]\delta(\nu_y)\right\}, \qquad (1)$$

where $*$ denotes convolution, $\delta\nu$ is the lateral dimension of the pixel and $\delta(\cdot)$ is the Dirac impulse function. In addition the relation

$$\sum_{i=1}^{3} W_i = 1 \qquad (2)$$

must be fulfilled.

Let $h(x,y)$ be the inverse Fourier transform of $H(\nu_x,\nu_y)$. We then have

$$h(x,y)=\int_{-\infty}^{\infty}\int_{-\infty}^{\infty}H(\nu_x,\nu_y)\exp\left[\mathrm{i}2\pi(x\nu_x+y\nu_y)\right]\mathrm{d}\nu_x\,\mathrm{d}\nu_y. \tag{3}$$

Thus, one obtains

$$\begin{aligned}h(x,y)=(\delta\nu)^2\operatorname{sinc}(\delta\nu y)\sum_m\sum_n\Bigg[&W_1\operatorname{sinc}(W_1\,\delta\nu\,x)\exp\left(-\mathrm{i}2\pi x\,\delta\nu\frac{W_2+W_3}{2}\right)\\&+\exp\left(\frac{\mathrm{i}2\pi}{3}\right)W_2\operatorname{sinc}(W_2\,\delta\nu\,x)\exp\left(\mathrm{i}2\pi x\,\delta\nu\frac{W_1-W_3}{2}\right)\\&+\exp\left(\frac{\mathrm{i}4\pi}{3}\right)W_3\operatorname{sinc}(W_2\,\delta\nu\,x)\exp\left(\mathrm{i}2\pi x\,\delta\nu\frac{W_1-W_2}{2}\right)\Bigg]\\&\times\exp\left[\mathrm{i}2\pi\,\delta\nu\,(xm+yn)\right],\end{aligned} \tag{4}$$

where $\operatorname{sinc}(x)$ is defined as

$$\operatorname{sinc}(x)=\frac{\sin(\pi x)}{\pi x}. \tag{5}$$

As an on-axis element, we restrict our interest only to regions of (x,y) corresponding to $x,y\ll 1/\delta\nu$. Therefore

$$\delta\nu\,x\ll 1,\quad \delta\nu\,y\ll 1, \tag{6}$$

and, as a result,

$$\operatorname{sinc}(W_i\,\delta\nu\,x),\operatorname{sinc}(W_i\,\delta\nu\,y)\approx 1,\quad \exp(\mathrm{i}2\pi x\,\delta\nu)\approx 1. \tag{7}$$

Equation (4) now becomes

$$\begin{aligned}h(x,y)\approx\text{constant}\sum_m\sum_n&\left[W_1+W_2\exp\left(\frac{\mathrm{i}2\pi}{3}\right)+W_3\exp\left(\frac{\mathrm{i}4\pi}{3}\right)\right]\\&\times\exp\left[\mathrm{i}2\pi\,\delta\nu\,(xm+yn)\right]\end{aligned} \tag{8}$$

or, in equivalent representation,

$$\begin{aligned}h(x,y)\approx\text{constant}\sum_m\sum_n&\left(W_1-0.5(W_2+W_3)+\mathrm{i}\frac{3^{1/2}}{2}(W_2-W_3)\right)\\&\times\exp\left[\mathrm{i}2\pi(xm+yn)\,\delta\nu\right].\end{aligned} \tag{9}$$

In a discrete system, the filter $H(\nu_x\nu_y)$ should represent an arbitrary complex distribution which in cell (m,n) is given by

$$H(m\,\delta\nu,n\,\delta\nu)=A_{m,n}\exp(\mathrm{i}\phi_{m,n}) \tag{10}$$

The Fourier integral of equation (3) is then transformed to a summation:

$$h(x,y)\approx\text{constant}\sum_m\sum_n H(m\,\delta\nu,n\,\delta\nu)\exp\left[\mathrm{i}2\pi(xm+yn)\,\delta\nu\right]. \tag{11}$$

Therefore

$$h(x,y) \approx \text{constant} \sum_m \sum_n A_{m,n} \exp(\mathrm{i}\phi_{m,n}) \exp[\mathrm{i}2\pi(xm + yn)\,\delta\nu]. \tag{12}$$

A comparison between equations (9) and (12) yields that the amplitude and the phase of each cell can be determined uniquely by the values of W_1, W_2 and W_3 according to

$$\begin{bmatrix} 1 & -\frac{1}{2} & -\frac{1}{2} \\ 0 & \frac{3^{1/2}}{2} & -\frac{3^{1/2}}{2} \\ 1 & 1 & 1 \end{bmatrix} \begin{bmatrix} W_1 \\ W_2 \\ W_3 \end{bmatrix} = \begin{bmatrix} \mathrm{Re}[A_{m,n} \exp(\mathrm{i}\phi_{m,n})] \\ \mathrm{Im}[A_{m,n} \exp(\mathrm{i}\phi_{m,n})] \\ 1 \end{bmatrix} \tag{13a}$$

or equivalently

$$\begin{bmatrix} W_1 \\ W_2 \\ W_3 \end{bmatrix} = \begin{bmatrix} \frac{2}{3} & 0 & \frac{1}{3} \\ -\frac{1}{3} & \frac{3^{1/2}}{3} & \frac{1}{3} \\ -\frac{1}{3} & -\frac{3^{1/2}}{3} & \frac{1}{3} \end{bmatrix} \begin{bmatrix} \mathrm{Re}[A_{m,n} \exp(\mathrm{i}\phi_{m,n})] \\ \mathrm{Im}[A_{m,n} \exp(\mathrm{i}\phi_{m,n})] \\ 1 \end{bmatrix}. \tag{13b}$$

Note that the above-described method reconstructs the Fourier transform of the encoded function in the zero-diffraction-order direction. Although the proposed analysis is based on a Fourier transform relation, other optical transformations such as Fresnel or fractional Fourier transformation can be applied as well.

3. Error and efficiency calculations

The proposed approach is based on the approximations described in equation (6). However, these approximations result in some error and therefore performance reduction is occurred. The main drawback of the encoding procedure is the fact that there is a spatial shift between the three different phases encoding the amplitude and phase of each cell. If the three phases could have been superposed, as in interferometric set-up, there could be less performance reduction. It is well known that the Fourier transform of a shifted object contains an additional linear phase factor. These phases are the terms $\exp[-\mathrm{i}2\pi x\,\delta\nu(W_2 - W_3)/2]$, $\exp[\mathrm{i}2\pi x\,\delta\nu(W_1 - W_3)/2]$ and $\exp[\mathrm{i}2\pi x\,\delta\nu(W_1 + W_2)/2]$ in equation (4). Better performance would be obtained if these terms were eliminated. Unfortunately, these terms cannot be pre-compensated since they influence differently the whole reconstructed plane. Other error sources are the three different sinc functions multiplying the phase terms, namely $\mathrm{sinc}(W_1\,\delta\nu X)$, $\mathrm{sinc}(W_2\,\delta\nu X)$, $\mathrm{sinc}(W_3\,\delta\nu X)$ which again cannot be pre-compensated. Although those terms are less harmful than the previous terms because they do not involve phase factors, some damage still occurred.

In order to evaluate the significance of the error, a specific example is discussed, assuming a specific cell (m,n) with values of $A_{m,n} = \frac{1}{2}$ and $\phi_{m,n} = 0$. According to the proposed encoding method, the width values should be set to $W_1 = \frac{2}{3}$, $W_2 = W_3 = \frac{1}{6}$. The reconstructed object $h(x,y)$ is expected within the window $|x|\,\delta\nu \leqslant \frac{1}{2}$. If one takes into account the additional phase and sinc terms

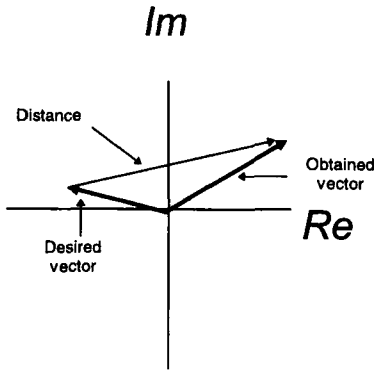

Figure 4. The distance expression.

and calculates from these width values the amplitude and the phase, it turns out that, while in the middle of the reconstruction area ($x = 0$) the values are still the same, in the edges ($x = \pm 1/(2\,\delta\nu)$) the obtained values are $A_{m,n} = 0.555$ and $\phi_{m,n} - 0.215\pi$ which is rather a large error. As one can see, the error is a function of the x coordinate. At $x = 0$ there is no error and at $x = \pm 1/(2\,\delta\nu)$ the error is maximal.

In order to decrease the undesired error terms it is recommended to use the oversampling approach. Practically, the best way to increase the oversampling is to surround the original object by zeros, which is equivalent to reducing $\delta\nu$. The oversampling factor is $P = \delta\nu\, u_{\max}$ when $u_{\max}$ is the maximal output window, and $\delta\nu$ is the hologram cell size. Therefore, the reconstructed image will be obtained at $|x| \leqslant 1/(2\,\delta\nu\, p)$. Assuming for instance that $P = 2$ and using the previous example, the values obtained are $A_{m,n} = 0.439$ and $\phi_{m,n} = -0.143\pi$, which is a significant improvement in both phase and amplitude compared with the $P = 1$ case.

Table 1 provides a summary of the expected performances of the proposed approach. This summary is based on the examination of three amplitude values $A_{m,n} = 0.1$, $A_{m,n} = 0.3$ and $A_{m,n} = 0.5$ (which is the maximal amplitude value allowed in this method, as will be explained) and two phase values $\phi_{m,n} = 0.2\pi$, and $\phi_{m,n} = 1.4\pi$. The *maximal* deviation from these values (which occurred at the edges) was checked for $P = 1$, 2, 4, 8 and 16. The important parameter in this table is the distance parameter defined (according to the law of cosines) as

$$\text{distance} = [A^2_{\text{obtained}} + A^2_{\text{desired}} - 2A_{\text{obtained}}A_{\text{desired}} \cos(\phi_{\text{obtained}} - \phi_{\text{desired}})]^{1/2}. \quad (14)$$

This parameter reflects accurately the deviation of the obtained values from the desired values. It can be seen that, if $P = 16$ is used, for high amplitude values the distance is less than 5% of the desired amplitude, while for low amplitude values the distance is more than 35% (see last row of table 1). However, one must keep in mind that these distance values are the maximal deviation values possible and the average values are much smaller. In fact, in the centre of the reconstruction area, no error occurred. Therefore, this method can yield good results, as can be seen in the next section by the computer simulations.

Another important aspect that influences the performances is the quantization problem. In order to perform the proposed encoding procedure properly, a high spatial bandwidth is needed. The evaluation of a large number of computer

Table 1. Performance evaluation. (All amplitude and phase values are for pixels at the edge region of the image which are excepted to be the pixels with maximal error. P is the oversampling factor. The distance is computed using equation (14).)

		$A_{desired} = 0.1$		$A_{desired} = 0.3$		$A_{desired} = 0.5$	
		$\phi_d = 0.2\pi$	$\phi_d = 1.4\pi$	$\phi_d = 0.2\pi$	$\phi_d = 1.4\pi$	$\phi_d = 0.2\pi$	$\phi_d = 1.4\pi$
$P = 1$	Obtained amplitude	0.305	0.398	0.287	0.6	0.284	0.657
	Obtained phase	-0.336π	1.658π	-0.353π	1.610π	-0.388π	1.549π
	Distance	0.331	0.337	0.448	0.406	0.638	0.308
$P = 2$	Obtained amplitude	0.232	0.321	0.235	0.472	0.286	0.631
	Obtained phase	-0.262π	1.623π	-0.125π	1.557π	-0.143π	1.504π
	Distance	0.241	0.252	0.267	0.2517	0.443	0.224
$P = 4$	Obtained amplitude	0.146	0.219	0.242	0.390	0.366	0.571
	Obtained phase	-0.172π	1.578π	0.045π	1.503π	0.131π	1.462π
	Distance	0.140	0.144	0.142	0.142	0.162	0.125
$P = 8$	Obtained amplitude	0.106	0.159	0.263	0.343	0.432	0.516
	Obtained phase	-0.002π	1.527π	0.128π	1.460π	0.71π	1.433π
	Distance	0.070	0.077	0.073	0.0741	0.080	0.055
$P = 16$	Obtained amplitude	0.098	0.130	0.279	0.284	0.462	0.508
	Obtained phase	0.08π	1.478π	0.167π	1.423π	0.188π	1.417π
	Distance	0.037	0.040	0.036	0.0265	0.042	0.028

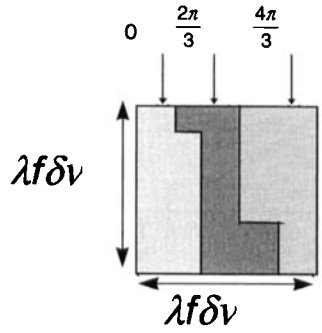

Figure 5. The two-dimensional top view of a cell.

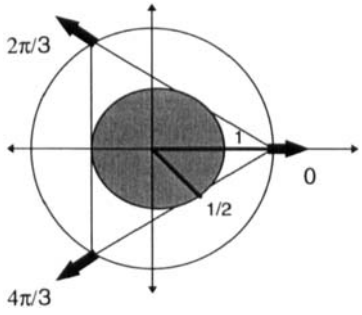

Figure 6. Efficiency calculation.

simulations and performances show that the usage of more than 50 pixels per cell (m, n) is recommended. Therefore, the needed resolution is 50 times finer than the cell's resolution. As an example, one can use a filter of 2 cm width with 64 original pixels. After using the oversampling factor of 16 and allowing 50 pixels per cell it turns out that the minimal resolution should be less than 0.5 μm, which may cause manufacture difficulties. The solution for this problem is to use a two-dimensional configuration in which the normalized area of subregion i is proportional to W_i. The top view of one cell in the two-dimensional configuration can be seen in figure 5. The use of the two-dimensional configuration and 49 pixels per cell increases the pixel's spatial degrees of freedom by a factor of seven. If the spatial bandwidth is M pixels per cell in the one-dimensional case, the two-dimensional configuration gives M^2 pixels per cell. In addition, the two-dimensional configuration can decrease the error by spreading the phase values in the entire cell.

In order to be able to encode any possible information, the amplitude information must be normalized. The maximal allowed amplitude value is the radius of the inner circle which is bounded by the triangle as shown in figure 6. Therefore $A_{\max}$ should be set to $\frac{1}{2}$ instead of 1 if one needs to avoid any error in the amplitude, because the above 100% light efficiency is not obtained. The maximal possible light intensity efficiency is given by the squared value of $A_{\max}$ or equivalently by the relation between the area of the inner and the outer circles (the outer circle is the circle which bounds the triangle, as shown in figure 6). Hence, the efficiency is given by

$$\eta = A_{\max}^2 = 0.25. \tag{15}$$

Table 2. Light efficiency against the number of phase levels.

Number of phases	Light efficiency
3	0.25
4	0.5
5	0.65
6	0.75
7	0.81
8	0.85
9	0.88
10	0.90
11	0.92
12	0.93
13	0.94
14	0.95
15	0.95
16	0.96

This value is rather low; however, it is much more than that given by the amplitude approach suggested by Burckardt in which this value must be multiplied by the amplitude grating efficiency which cannot exceed 0.1.

If one allows an amplitude error for some specific vectors (those between $\frac{1}{2}$ and 1), 100% efficiency can be obtained. Compromise between these two extremes are possible as well.

Alternatively, the efficiency can be increased by using more than three partitions. The maximal allowed amplitude can be found from

$$A_{\max} = \cos\left(\frac{180^\circ}{n}\right), \tag{16}$$

where n is the number of the partitions (phases). Therefore, the light efficiency is given by

$$\eta = A_{\max}^2 = \left[\cos\left(\frac{180^\circ}{n}\right)\right]^2. \tag{17}$$

The light efficiencies for several values of n are given in table 2. This table indicates the production complexity against light-efficient trade-off.

4. Computer simulations

In order to estimate the performances of the proposed approach, several computer simulations were carried out. The simulations were based on a two-dimensional filter structure with total bandwidth of 81 pixels per cell. The reconstruction quality can be estimated by using the mean squared error (MSE) criterion defined as

$$\mathrm{MSE} = \sum_m \sum_n |h_{m,n}^{\text{desired}} - h_{m,n}^{\text{obtained}}|^2, \tag{18}$$

where the intensity of both the desired and the obtained functions should be normalized according to

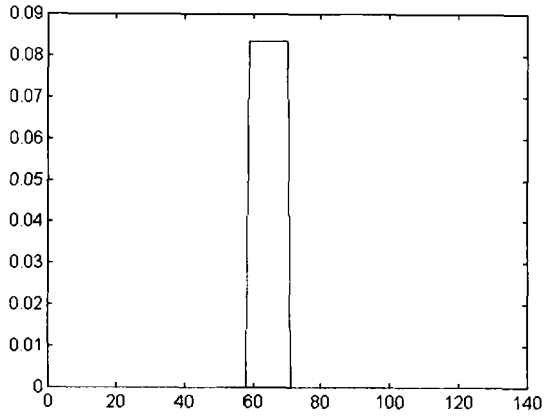

(*a*)

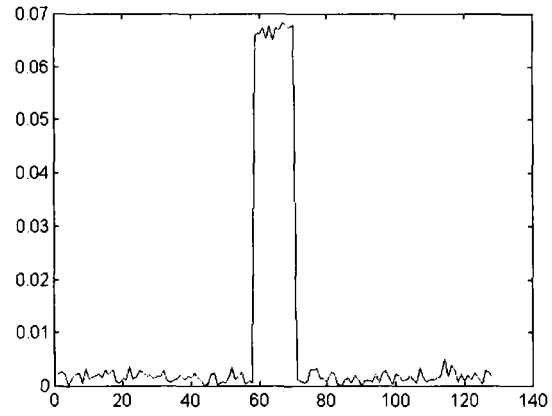

(*b*)

Figure 7. (*a*) The one-dimensional top hat to be reconstructed. (*b*) The amplitude reconstruction of (*a*) (the on-axis region).

$$\sum_m \sum_n |h_{m,n}^{\text{desired}}|^2 = \sum_m \sum_n |h_{m,n}^{\text{obtained}}|^2 = 1. \tag{19}$$

Figue 7 (*a*) shows a one-dimensional top-hat object ($P = 10$ was used). The on-axis region of the reconstruction is shown in figure 7 (*b*). The MSE value obtained is 0.0041. A two-dimensional demonstration is given in figure 8. There, the amplitude shape of the latter H is used. The desired shape is shown in figure 8 (*a*) (this time with $P = 4$). The on-axis region of the reconstruction is shown in figure 8 (*b*). The MSE value obtained is 0.0091.

In addition to the amplitude objects shown in figures 7 and 8, two phase-only objects were tested. The tested objects were the same as the amplitude objects, but the amplitude levels 0 and 1 were replaced by phase levels of 0 and π. For example, the letter H was rebuilt by π-phase bars surround by 0-phase values. The on-axis region of the reconstructions of figures 7 (*a*) and 8 (*a*) are shown in figures 9 and 10 respectively. MSE values of 0.0051 and 0.0190 respectively were obtained. The phase elements were composed of a constant amplitude in the whole region.

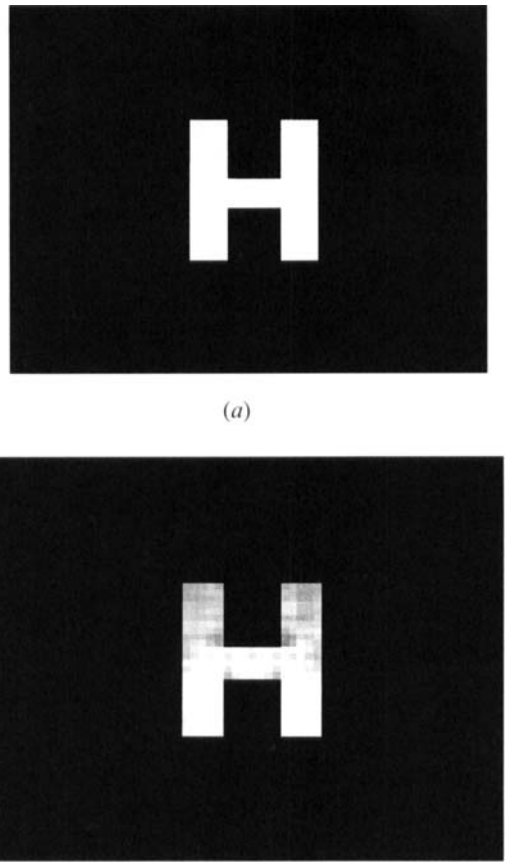

(*a*)

(*b*)

Figure 8. (*a*) The letter H to be reconstructed. (*b*) The amplitude reconstruction of (*a*) (the on-axis region).

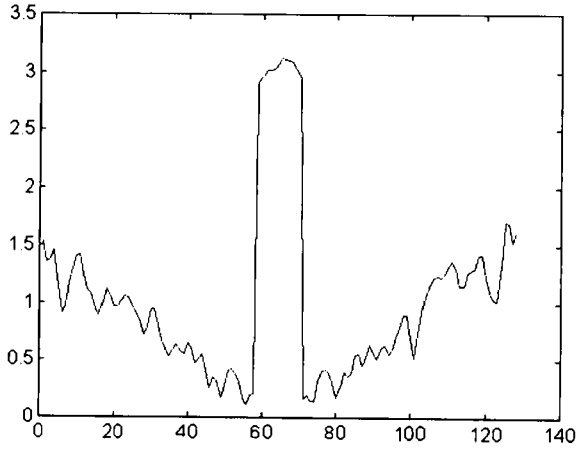

Figure 9. The phase reconstruction of the phase-only top-hat object.

Figure 10. The phase reconstruction of the phase-only H object.

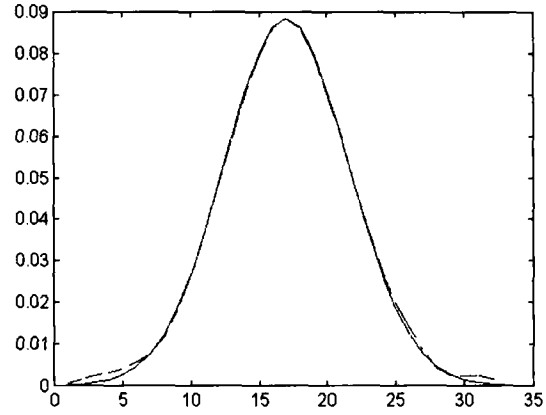

Figure 11. The Gaussian amplitude (——), original amplitude; (— —) reconstructed amplitude.

Therefore no oversampling factor were used. This is the reason for the phase deviation that became more severe towards the edges, as expected from the error analysis.

The ability of the proposed approach to handle complex functions which contains both phase and amplitude information was investigated by the reconstruction of a complex Gaussian function. Figure 11 gives the desired amplitude (solid curve) and the reconstructed amplitude (broken curve). Figure 12 depicts the same for the phase information. The overall MSE value is 0.002.

5. Conclusions

A new approach for encoding arbitrary phase and amplitude distributions has been proposed. The new technique expands the variety of solutions for performing on-axis computer-generated holography. The suggested method is based on a phase-only filter which contains only three different phase values; therefore only two identical production steps (e.g. etching) are needed. The hologram mask was designed to reconstruct the image around the zero diffraction order and therefore

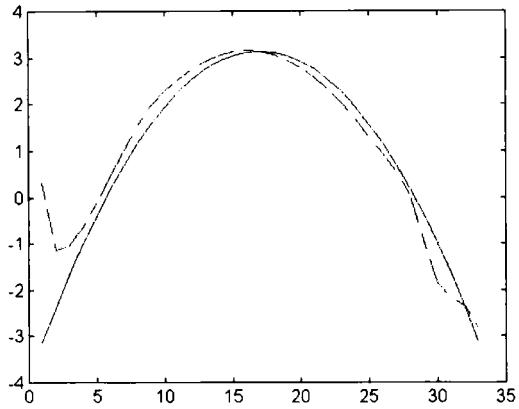

Figure 12. The Gaussian phase: (——), original phase; (— —) reconstructed phase.

is less sensitive to variations in the wavelength of the illuminating source. This approach addresses the cases where the combination of fast computation and a small number of etch levels is needed. Increasing the number of etch levels results in better light efficiency.

This proposed approach offers some potential for dynamic elements that are based on spatial light modulators. The obtained elements can be used in a variety of applications such as optical correlators, displays and beam-shaping devices. Computer simulations have shown that the method can cope successfully in reconstructing different types of object, as expected from the theoretical background.

Acknowledgments

The authors acknowledge a fruitful discussion with Emanul Marom and Gal Shabtay. Uriel Levy acknowledge the Israeli Ministry of Science and the Arts for financial support.

References

[1] Brown, G. R., and Lohmann, A. W., 1966, *Appl. Optics*, **6,** 967.
[2] Lohmann, A. W., and Paris, D. P., 1967, *Appl. Optics*, **6,** 1739.
[3] Lee, W. H., 1970, *Appl. Optics*, **9,** 687.
[4] Burckhardt, C. B., 1970, *Appl. Optics*, **9,** 1949.
[5] Hsueh, C. K., and Sawchuck, A. A., 1978, *Appl. Optics*, **17,** 3874.
[6] Gallagher, N. C., and Bucklew, J. A., 1980, *Appl. Optics*, **19,** 4266.
[7] Matic, R. M., and Hensen, E. W., 1982, *Appl. Optics*, **21,** 2304.
[8] Lesem, L. B., Hirsch, P. M., and Jordan, J. A., Jr, 1969, *IBM Jl Res. Dev.*, 150.
[9] Kirk, J. P., and Joens, A. L., 1971, *J. opt. Soc. Am.* A, **61,** 1024.
[10] Florence, J. M., and Juday, R. D., 1991, *Proc. SPIE*, **1558,** 487.
[11] Mendlovic, D., Shabtay, G., Levi, U., Zalevsky, Z., and Marom, E., 1997, *Appl. Optics*, **36,** 8427.
[12] Weissbach, S., Wyrowski, F., and Bryngdahl, O., 1989, *Optics Commun.*, **72,** 37.
[13] Wyrowski, F., 1990, *J. opt., Soc. Am.* A, **7,** 961.
[14] Yoshikawa, N., and Yatagai, T., 1994, *Appl. Optics*, **33,** 863.